Journal of Materials Chemistry

Cite this: *J. Mater. Chem.*, 2011, **21**, 16420

www.rsc.org/materials

PAPER

Fibrous-structured magnetic and mesoporous Fe_3O_4/silica microspheres: synthesis and intracellular doxorubicin delivery

Shili Gai,[a] Piaoping Yang,*[a] Ping'an Ma,[b] Dong Wang,[a] Chunxia Li,[b] Xingbo Li,[a] Na Niu[a] and Jun Lin[b]

Received 17th July 2011, Accepted 17th August 2011
DOI: 10.1039/c1jm13357h

A novel, fibrous-structured bifunctional (magnetic and mesoporous) Fe_3O_4/silica microsphere was successfully synthesized through a simple and economical self-assembled process in which hydrophobic 9 nm-Fe_3O_4 nanocrystals were directly used without modifications. The obtained material is performed as a drug delivery carrier to investigate the *in vitro* and intracellular delivery properties of doxorubicin hydrochloride (DOX). X-Ray diffraction (XRD), scanning electron microscopy (SEM), transmission electron microscopy (TEM), N_2 adsorption/desorption, Fourier transform infrared spectroscopy (FT-IR), and superconducting quantum interference device (SQUID) were employed to characterize the composite. The results reveal that the novel composite exhibits typical mesoporous structure, narrow size distribution, good monodispersity, and superparamagnetic features. Notably, confocal laser scanning microscopy (CLSM) images indicate that the DOX-loaded sample could deliver DOX into the nuclei of HeLa cells to kill cells. Also, MTT assay confirms that the DOX-loaded sample leads to pronounced and efficient cytotoxic effects to L929 fibroblast cells, even similar to that of free DOX at high concentrations, whereas the pure material is non-toxic. Therefore, the novel material is expected to have potential application for targeted cancer therapy.

1. Introduction

During the past decade, iron oxide-based magnetic mesoporous materials have attracted growing attention not only due to their unique magnetic responsivity, low toxicity,[1] biocompatibility, biodegradability and tunable mesoporous structures, but also for their great potential applications in the fields of magnetic bioseparations,[2] heterogeneous catalysis,[3] enzyme immobilization,[4] targeted drug delivery,[5] and environmental technology.[5d] Currently, there are mainly two general ways to synthesize iron oxide-based magnetic mesoporous materials. One is to prepare pure iron oxide mesoporous/hollow spheres.[6] However, the pure iron oxide mesoporous/hollow spheres possess low surface area along with small pore volume, which dramatically limit their applications as functional porous materials. Besides, pure iron oxide materials are prone to aggregation and rapid biodegradation when they are exposed to biological systems.[7] Thereby, the other way to design iron oxide-based magnetic mesoporous composite materials composed of iron oxide particles and a mesoporous matrix (such as silica,[8] carbon,[9] polymer,[10] collagen,[11] and lipid[12]) has been the focus of many researchers. Among these matrix materials, amorphous mesoporous silica has been considered to be an ideal candidate for biological applications owing to its non-toxic nature, tunable pore size, very high surface area and pore volume.[13]

Recently, a significant breakthrough has been achieved on the synthesis of monodisperse iron oxide nanocrystals (NCs) with superparamagnetism, high crystallinity, narrow size distributions, and dimensions on the order of 10 nm by high-temperature thermolysis of organometallic species.[14] The high-quality iron oxide NCs are highly desirable for function-specific biological applications. However, the products obtained from the above approach are organic-soluble, which greatly limits their applications in biological fields. Although several strategies have been developed to transfer the hydrophobic NCs from non-polar solvent to water, including ligand exchange,[15] surface modification,[8c,16] and encapsulating magnetic NCs in a silica shell,[17] these procedures need expensive and/or toxic organic agents with very complicated and time-consuming synthetic steps. Therefore, the development of a facile and low-cost approach which directly utilizes the high-quality hydrophobic iron oxide NCs to prepare magnetic and mesoporous silica materials is still a challenging and important research topic at the present time.

In this contribution, we report a very simple and economical mass-production self-assembled process in which hydrophobic iron oxide (9 nm-Fe_3O_4) NCs were directly used for the formation of magnetic and mesoporous silica material. Interestingly, the as-prepared material consists of fascinating fibrous-structured microspheres with high surface area, and has an average particle diameter of 300 nm which is within the applicable size for

[a]*Key Laboratory of Superlight Materials and Surface Technology, Ministry of Education, Harbin Engineering University, Harbin, 150001, P. R. China. E-mail: yangpiaoping@hrbeu.edu.cn*
[b]*State Key Laboratory of Rare Earth Resources Utilization, Changchun Institute of Applied Chemistry, Chinese Academy of Sciences, Changchun, 130022, Beijing, 100049, P. R. China. E-mail: jlin@ciac.jl.cn*

drug and gene delivery.[18] Most importantly, the synthetic strategy presented here may have a good prospect for large-scale application and provide an effective route to synthesize other multifunctional silica materials using different hydrophobic nanocrystals. In addition, pure fibrous mesoporous silica microspheres (FMSMs) without the addition of hydrophobic Fe_3O_4 NCs have also been synthesized by the same process for comparison. The result shows that the introduction of the hydrophobic Fe_3O_4 is favorable to form high surface area, large pore size, and reduce the diameter of the product. The influence of the hydrophobic iron oxide is discussed and a possible mechanism is proposed.

In order to design an ideal material for therapeutics, the unintentional toxicity and biocompatibility of the fibrous-structured magnetic and mesoporous Fe_3O_4/FMSMs microspheres have been monitored by MTT assay. Furthermore, doxorubicin hydrochloride (DOX), which is one of the most employed anthracycline antitumor drugs in clinical practice nowadays,[19] was used as a model drug to investigate the *in vitro* and intracellular release properties of Fe_3O_4/FMSMs sample.

2. Experimental section

2.1. Method

Synthesis of Fe_3O_4/FMSMs. All chemicals were of analytical grade and used without further purification. Fe_3O_4 NCs with a uniform diameter of 9 nm were obtained by a high-temperature thermolysis procedure using 0.105 mmol of iron-oleate complexes in a solution of oleic acid surfactant and 1-octadecene solvent.[14a] The obtained oleate-capped Fe_3O_4 NCs were dissolved in 30 mL of cyclohexane. Then, 2.7 mL of tetraethyl orthosilicate (TEOS) and 1.5 mL of pentanol were added to get solution A. 0.95 g of cetyltrimethylammonium bromide (CTAB) and 0.6 g of urea were dissolved in 30 mL of deionized water to form solution B. Subsequently, solution B was mixed with solution A under vigorous stirring. After stirring for 30 min, the mixture was transferred to a 100 mL Teflon-lined autoclave and heated at 120 °C for 4 h. The obtained products were washed with acetone and deionized water in sequence, and dried in air for 24 h. At last, the sample was calcined from room temperature to 550 °C with a heating rate of 1 °C min^{-1} and maintained at this temperature for 6 h. In this way, the fibrous-structured magnetic and mesoporous microspheres (denoted as Fe_3O_4/FMSMs) were obtained. The formation process of Fe_3O_4/FMSMs was depicted in Scheme 1. For comparison, pure fibrous mesoporous silica microspheres (FMSMs) were prepared in a similar process, except for using Fe_3O_4 NCs.

***In vitro* drug release.** Typically, 30 mg of Fe_3O_4/FMSMs was added to 5 mL of phosphate buffer solution (PBS, pH = 7.4) of DOX with a concentration of 0.5 mg mL^{-1} at room temperature, and soaked for 24 h under stirring in dark conditions. The DOX-loaded sample was separated by centrifugation, and denoted as DOX–Fe_3O_4/FMSMs. The *in vitro* delivery test was performed by immersing the DOX–Fe_3O_4/FMSMs sample in 10 mL of PBS under gentle stirring in dark conditions, and the immersing temperature was kept at 37 °C. At selected time intervals, buffer solution was taken and immediately replaced with an equal volume of fresh PBS. The amount of released DOX in the taken PBS was measured by UV-vis spectrophotometer at 490 nm.

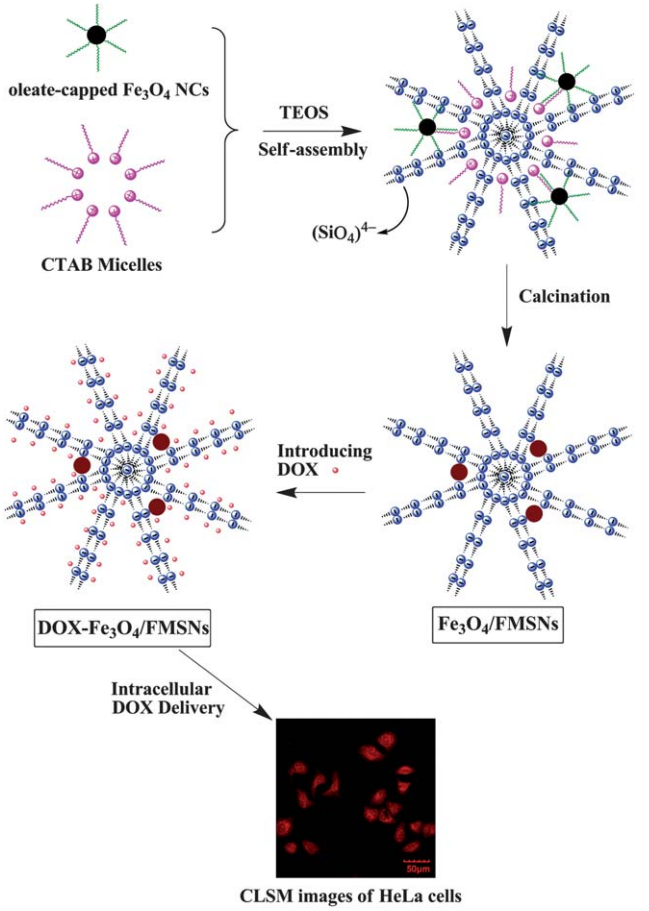

Scheme 1 Schematic illustration showing the possible formation mechanism of Fe_3O_4/FMSMs by self-assembled process, and the subsequent drug loading and intracellular delivery process.

Intracellular release of DOX. HeLa (human adenocarcinoma) cells were cultured in 6-well plates (2.5×10^4 cells per well) for 24 h. After being rinsed twice with PBS, DOX–Fe_3O_4/FMSMs were added into each well at a concentration of 20 μg mL^{-1}. After being incubated for 10 min, 1 h, 3 h, and 6 h at 37 °C, the cells were rinsed by PBS and dyed with 10 μg mL^{-1} of Hoechst 33324 for 10 min. Finally, the cells were washed twice with PBS and observed using confocal laser scanning microscopy (CLSM). In addition, SKOV3 (human ovarian carcinoma) cells were cultured in a humidified atmosphere of 5% CO_2 at 37 °C for the cell nucleus assays using microscopic images. The concentration of DOX–Fe_3O_4/FMSMs is 30 μg mL^{-1}.

MTT cytotoxicity assay. MTT (3-(4,5-dimethylthiazol-2-yl)-2, 5-diphenyltetrazolium bromide) cell assay was used on the Vero cell line to evaluate the biocompatibility of DOX, DOX–Fe_3O_4/FMSMs and Fe_3O_4/FMSMs. In a typical procedure, 5000–6000 L929 fibroblast cells were plated in 200 μL media per well in a 96-well plate, and 8 wells were left empty for blank control, then incubated (37 °C, 5% CO_2) overnight to allow the cells to attach to the wells. Fe_3O_4/FMSMs were sterilized by ultraviolet

irradiation for 2 h, and then serial dilutions of the particles at concentrations of 0.78, 1.56, 3.12, 6.24, 12.48, and 24.96 μg mL^{-1} were added to the culture wells to replace the original culture medium and incubated for another 24 h in 5% CO_2 at 37 °C. 5 mg mL^{-1} stock solution of MTT was prepared in PBS and 20 μL of this stock solution was added to each well containing different amounts of Fe_3O_4/FMSMs. The plate was subsequently incubated at 37 °C for another 4 h covered with aluminium foil for protection from light. During this period, viable cells reduce MTT to formazan pigment, which can be dissolved by dimethyl sulfoxide (DMSO). After incubation, 100 μL of acidified isopropanol was added to each well, and placed on a shaking table of 150 rpm, 5 min, to thoroughly mix the formazan into the solvent. The absorbance of the suspension was recorded under a microplate reader at 570 nm.

2.2. Characterization

X-Ray diffraction (XRD) measurements were carried out with Rigaku-Dmax 2500 diffractometer using Cu-Kα radiation (λ = 0.15405 nm). The morphologies of the as-prepared samples were inspected on a field emission scanning electron microscope (FESEM, S4800, Hitachi). Transmission electron microscopy (TEM) and high-resolution transmission electron microscopy (HRTEM) micrographs were obtained from a FEI Tecnai G^2 S-Twin transmission electron microscope with a field emission gun operating at 200 kV to elucidate the dimensions and the structural details of the particles. Inductively coupled plasma (ICP) measurement (Thermo iCAP 6000 ICPOES) was performed on the sample to determine the exact doping level of Fe_3O_4 in FMSMs. ^{29}Si MAS/NMR experiments were carried out at the frequency of 400 MHz on a Bruker NMR spectrometer. FT-IR spectra were measured on a Perkin-Elmer 580B IR spectrophotometer using the KBr pellet technique. N_2 adsorption/desorption isotherms were measured at a liquid nitrogen temperature (−196 °C) using a Micromeritics ASAP 2010 instrument. The specific surface area was calculated by the Brunauer–Emmett–Teller (BET) method. Magnetization measurements were performed on a MPM5-XL-5 superconducting quantum interference device (SQUID) magnetometer at 27 °C. The UV-vis absorption spectra values were measured on a TU-1901 spectrophotometer. Confocal laser scanning microscopy (CLSM) images were observed by confocal laser scanning microscope (Olympus, FV 1000). All the measurements were performed at room temperature.

3. Results and discussion

3.1. Formation, phase, morphology, and structure properties

A possible formation mechanism of Fe_3O_4/FMSMs by a self-assembled process is presented in Scheme 1. In the micro-emulsion system (mixture of solution A and B), the fibrous template molecules are assembled by cetyltrimethylammonium bromide (CTAB) micelles. And the oleate-capped Fe_3O_4 NCs are absorbed on the CTAB template *via* electrostatic interaction.

Simultaneously, in the available space among the fibrous template molecules, the negatively charged silicate molecules, produced by the hydrolysis and ionization of silica precursor (TEOS) with urea, are assembled along the free radial directions and the restricted tangential directions. Then, condensation of the self-assembled silicate leads to the crystallization of silica material with the absorbed Fe_3O_4 NCs and within the fibrous template molecules. Finally, under the condition of high temperature calcination, the CTAB template is burned out and the Fe_3O_4 NCs are fixed/embedded in the ordered silica fibers. In the protocol, the oleic acid ligands on the surface of the hydrophobic Fe_3O_4 NCs serve not only as the stabilizing agent, but also as the organic template (similar to CTAB) for the formation of mesopores in the self-assembled process.

Fig. 1A shows the XRD patterns of the pure Fe_3O_4 and as-prepared Fe_3O_4/FMSMs (with 1.7% Fe_3O_4 doping level). For Fe_3O_4/FMSMs, the broad band centered at 2θ = 22° can be assigned to the amorphous mesoporous SiO_2 (JCPDS No. 29-0085), corresponding to the pure FMSMs. The other diffraction peaks can be readily indexed to a face-centered cubic structural (*Fd3m* space group) magnetite (JCPDS No. 19-0629), which indicates that the material is composed of amorphous silica and crystalline magnetite. Fig. 1B–D gives the FE-SEM images of Fe_3O_4/FMSMs with different magnifications. From the low-magnification SEM image (Fig. 1B), it can be seen that the sample consists of monodisperse microspheres with an average particle diameter of 300 nm. The high-magnification SEM images (Fig. 1C,D) reveal that the sample exhibits interesting fibrous structure with dendrimeric fibers in the three-dimensional space.

The detailed morphological and structural features of Fe_3O_4/FMSMs were further examined by TEM. In Fig. 2A, the Fe_3O_4 NCs exhibit excellent monodispersity and uniform spherical shape with narrow size distribution (inset in Fig. 2A). The TEM images of Fe_3O_4/FMSMs (Fig. 2B–E) clearly show that the sample possesses interesting fibrous structure with the fixed/embedded Fe_3O_4 NCs which distribute in the center part of the Fe_3O_4/FMSMs. It also can be seen that the thickness of the well-defined silica fibers that come out from the center and distribute uniformly in all directions is 8–10 nm. In addition, the obvious lattice fringes of Fe_3O_4/FMSMs in the HRTEM image (Fig. 2F) can be associated with the fixed/embedded Fe_3O_4 NC. And the distance of 0.31 nm between the adjacent lattice fringes agrees

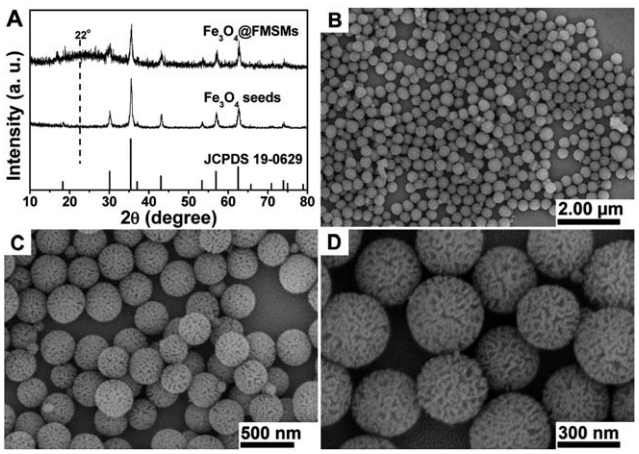

Fig. 1 (A) XRD patterns of oleate-capped Fe_3O_4 NCs and Fe_3O_4/FMSMs; (B) FE-SEM image and (C,D) magnified FE-SEM images of Fe_3O_4/FMSMs.

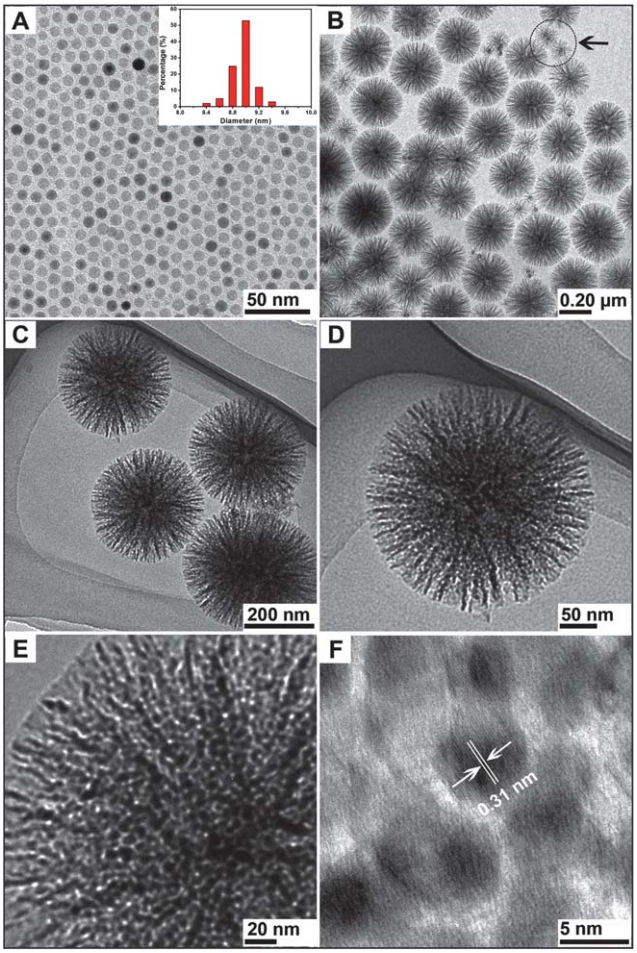

Fig. 2 (A) TEM image of 9 nm-Fe_3O_4; (B–E) TEM images with different magnifications, and (F) HRTEM image of Fe_3O_4/FMSMs.

with the d_{220} spacing (0.30 nm) of face-centered cubic structural magnetite, which is in good agreement with the wide-angle XRD results (Fig. 1A).

To study the influence of oleate-capped Fe_3O_4 on the size and dimension of the fibrous-structured microspheres, Fig. 3 gives the FE-SEM images and TEM images of Fe_3O_4/FMSMs and pure FMSMs. Obviously, the introduction of oleate-capped Fe_3O_4 is of benefit to form large pore size and long channel, and dramatically reduces the diameter of the particles from 700 nm to 300 nm, which proves the formation mechanism of Fe_3O_4/FMSMs in Scheme 1.

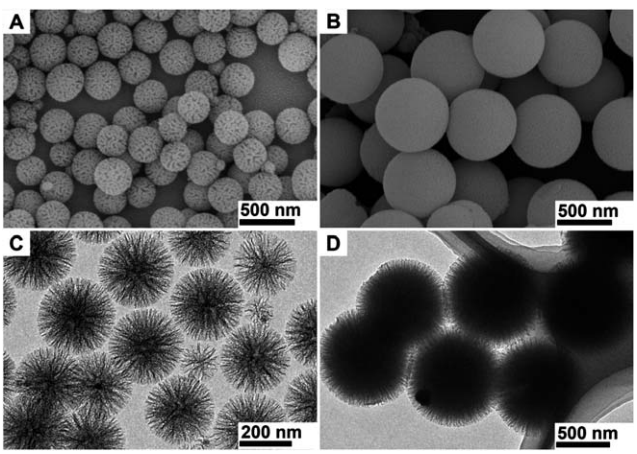

Fig. 3 FE-SEM images of (A) Fe_3O_4/FMSMs and (B) pure FMSMs; TEM images of (C) Fe_3O_4/FMSMs and (D) pure FMSMs.

The thermal stability of Fe_3O_4/FMSNs was examined by TG analysis (Fig. 4A). Only negligible weight loss (2.3%) assigned to the adsorbed water, hydroxyl groups and a small amount of oleic acids is observed up to 1200 °C, suggesting the high stability of the material. In the ^{29}Si CP/MAS NMR spectrum (Fig. 4B), a high resonance peak at −112 ppm and a weak shoulder at −101 ppm can be assigned to the surface silicon in Q^4 [$Si(OSi)_4$] and Q^3 [$(SiO)_3SiOH$] state,[20] respectively. Absence of signals at about −60 ppm indicates that no Si–C bonds are formed in the material.

N_2 adsorption/desorption isotherms of Fe_3O_4/FMSMs and DOX–Fe_3O_4/FMSMs (DOX-loaded sample) are shown in Fig. 5. It can be seen that both samples show similar IV isotherms and the typical H_1-hysteresis loops, suggesting the mesoporous nature of the two samples. The results also reveal that the loading of DOX molecules have not altered the basic pore structure of Fe_3O_4/FMSMs. The relatively wide pore size distributions (insets in Fig. 5) should be due to the unique porous structures with large pores in the outer surface and small pores in the inner surface. In comparison with the high BET surface area (340 m^2 g^{-1}), pore volume (0.733 cm^3 g^{-1}) and average pore size (10.6 nm) of Fe_3O_4/FMSMs, the BET surface area, pore volume and average pore size for DOX-loaded samples are markedly reduced to 131 m^2 g^{-1}, 0.431 cm^3 g^{-1} and 8.7 nm, further confirming the successful incorporation/adsorption of drug molecules into the mesoporous channels of Fe_3O_4/FMSMs.

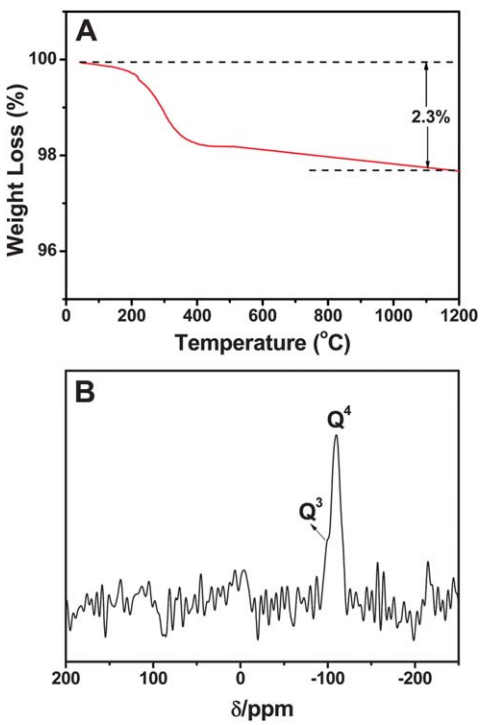

Fig. 4 (A) TG analysis and (B) ^{29}Si NMR spectrum of Fe_3O_4/FMSMs.

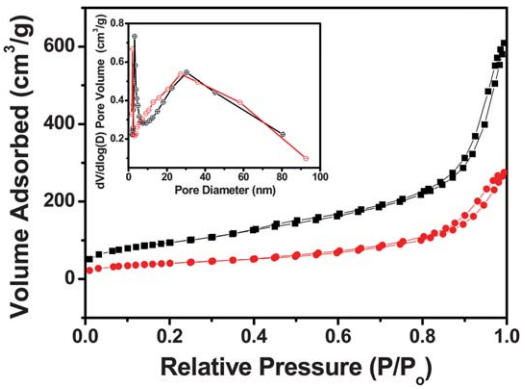

Fig. 5 N_2 adsorption/desorption isotherms of Fe_3O_4/FMSMs (black line) and DOX–Fe_3O_4/FMSMs (red line). Insets are their corresponding pore size distributions.

Fig. 6 presents the FT-IR spectra of Fe_3O_4/FMSMs, DOX–Fe_3O_4/FMSMs, and pure DOX. In Fig. 6A, for Fe_3O_4/FMSMs, several broad absorption bands assigned to OH (3435 cm^{-1}), Si–O–Si (1095 cm^{-1}), Si–OH (809 cm^{-1}), and Si–O (467 cm^{-1}) groups are detected, which can be attributed to the amorphous mesoporous silica.[21] The strong band of OH (3435 cm^{-1}) indicates that there are a large number of OH groups present on the surface, which are important for bonding drug molecules. Two characteristic absorption peaks at 1617 and 1579 cm^{-1} are ascribed to the stretching vibration of $\nu_{C=O}$ from the anthraquinone ring, and the peak at 994 cm^{-1} which can be attributed to C–O stretching of alcohol appears in pure DOX (Fig. 6C). And the couple of the peaks are also observed in DOX–Fe_3O_4/FMSMs (Fig. 6B), confirming the successful loading of DOX on Fe_3O_4/FMSMs. It can be attracted to a magnetic field while no residual magnetism is retained after the field is removed. The saturation magnetizations of Fe_3O_4/FMSMs and DOX–Fe_3O_4/FMSMs are measured to be 2.68 and 1.91 emu g^{-1}, respectively. Moreover, Fe_3O_4/FMSMs with homogeneous dispersion shows a response to the external magnetic field (Fig. 7B). It exhibits the good magnetic responsivity and redispersibility of Fe_3O_4/FMSMs, revealing the potential application for targeting and separation as a drug carrier.

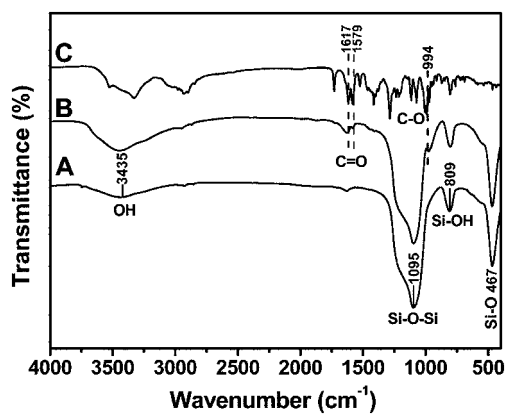

Fig. 6 FT-IR spectra of (A) Fe_3O_4/FMSMs, (B) DOX–Fe_3O_4/FMSMs and (C) pure DOX sample.

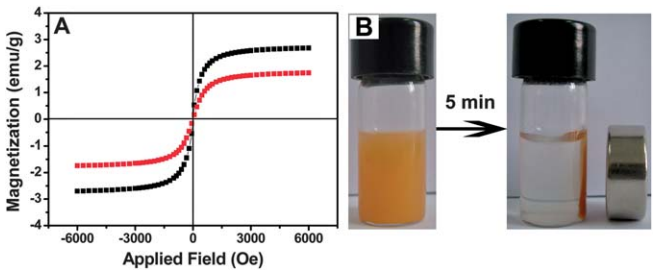

Fig. 7 (A) Magnetizations of Fe_3O_4/FMSMs (black line) and DOX–Fe_3O_4/FMSMs (red line) as a function of applied magnetic field measured at room temperature; (B) photograph of the separation process of Fe_3O_4/FMSMs by a magnet.

3.2. *In vitro* and intracellular release of DOX

As a candidate for a novel drug carrier, the drug storage and release properties of Fe_3O_4/FMSMs using DOX as a model drug are investigated. It is accepted that the DOX molecules are entrapped within the mesopores by an impregnation process and liberated *via* a diffusion-controlled manner. Therefore, the Si–OH groups on the mesoporous material surface should be important to form hydrogen bonds with the carboxyl groups in the drug molecules. In the release process, when the phosphate buffer solution (PBS) flowed inside the mesopores, the drug was dissolved slowly into PBS and diffused out from the composite along the mesoporous channels.

The *in vitro* drug release profile of DOX–Fe_3O_4/FMSMs in PBS as a function of the release time is given in Fig. 8A. As shown, the release of DOX was characterized by two distinct stages: a relatively rapid release over the first 1 h followed by a sustained release over 20 h. The initial fast release may be attributed to the rapid diffusion of the physically adsorbed drug molecules, which interact more weakly with the outer surfaces or near the pore entrances of the channels. Then the drug stored in the channels and adsorbed in the inner surfaces will dissolve after the longer-time penetration of the medium and diffuse along

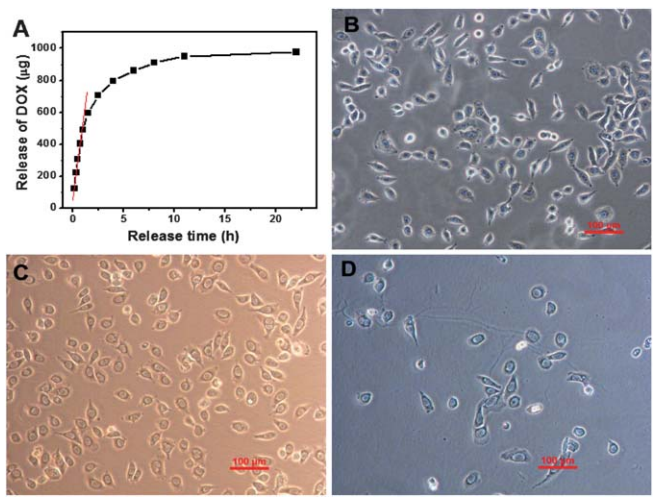

Fig. 8 (A) Drug-release profile for DOX–Fe_3O_4/FMSMs in PBS buffer; (B) the nucleus of bank SKOV3 cells; (C) the nucleus of SKOV3 cells incubated with DOX–Fe_3O_4/FMSMs for 8 h, and (D) for 24 h.

aqueous pathways into the medium. And the slow release of DOX can be due to the strong interaction between drug molecules and the hydrogen bonds on the material surface. It therefore can be inferred that the Fe_3O_4/FMSMs system possesses capability as a drug carrier for targeting systems in the drug delivery and disease therapy fields. Furthermore, to inhibit the tumor cell growth in tumor treatment, the initial burst of DOX release is preferable to achieve a sufficient initial dosage of the antitumor drug. For the cancer cells that survive the initial stage of the drug release, the sustained DOX release is necessary to prevent their further proliferation. Thus, the drug release performance of the carrier makes it a promising candidate for tumor therapy.

For the microscopic images of SKOV3 cells, compared with the normal morphology of the SKOV3 nucleus (Fig. 8B), expansion of the nuclear volume and fragmentation of the nucleus (karyorrhexis) occur after being treated with DOX–Fe_3O_4/FMSMs for 8 h (Fig. 8C), which are typical morphological features of cell apoptosis in an early stage. With 24 h of further incubation, a marked apoptosis in the majority of SKOV3 cells and cell contraction corresponding to a typical late apoptosis are observed (Fig. 8D). The results clearly reveal the activity of DOX with the mechanisms of killing tumor cells by DNA damage and topoisomerase II inhibition.[22] Thus, active preloading of DOX in DOX–Fe_3O_4/FMSMs can be proved. Moreover, the therapeutic effect of DOX–Fe_3O_4/FMSMs and the release of DOX at predetermined time points exhibit a similar trend within 24 h (Fig. 8A).

To further investigate the intracellular drug delivery and therapeutic effect of DOX–Fe_3O_4/FMSMs, DOX fluorescence in HeLa cell was examined using CLSM (Fig. 9). Incubated with DOX–Fe_3O_4/FMSMs, strong red fluorescence arising from DOX is observed both in the cell cytoplasm and cell nucleus, indicating that the DOX delivered by DOX–Fe_3O_4/FMSMs can pass through the cytomembrane, assemble in cytoplasm, then pass through the nucleus membrane and eventually assemble in nucleus to kill cells. Moreover, the intensity of red fluorescence is increased gradually in cells as the prolonging of incubation time, resulting from the sustained drug release property of DOX–Fe_3O_4/FMSMs. Thus, the effective therapy may result from the enhanced intracellular delivery and the protection of DOX extracellular by DOX–Fe_3O_4/FMSMs. This result indicates that Fe_3O_4/FMSMs may be a therapeutically effective drug delivery system for DOX delivery.

3.3. MTT cytotoxicity assay

Having confirmed the feasibility of using DOX–Fe_3O_4/FMSMs for cancer cell imaging, further study of the cellular cytotoxicity, a key factor in evaluating the potential application of the drug delivery system, was performed using MTT assay to examine the cell viability of Fe_3O_4/FMSMs and DOX–Fe_3O_4/FMSMs (Fig. 10). The anticancer drug DOX was used as a positive control in this experiment. For Fe_3O_4/FMSMs, more than 100% L929 fibroblast cells viability is observed under a varying concentration range, showing the satisfactory biocompatibility of the carrier, even at the highest concentration of 24.96 μg mL^{-1}. The results indicate that the sample is a non-toxic material and promising for biomedical applications.

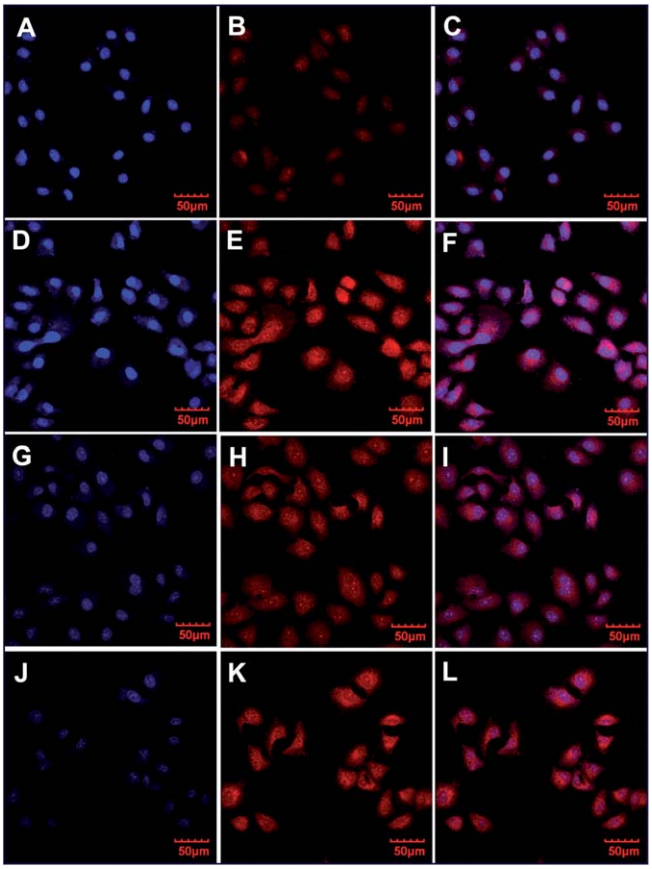

Fig. 9 Confocal laser scanning microscopy (CLSM) images of HeLa cells incubated with DOX–Fe_3O_4/FMSMs ([DOX] = 2 mM) for 10 min (A–C), 1 h (D–F), 3 h (G–I), and 6 h (J–L) at 37 °C. For each series, images from left to right can be classified to the nuclei of cells (blue, being dyed by Hoechst 33324), DOX fluorescence in cells (red), and the merged images of both above, respectively.

For DOX–Fe_3O_4/FMSMs, the viability of the fibroblast cell is higher than that of the free DOX, which may be caused by the lower amount (51%) of DOX released from DOX–Fe_3O_4/FMSMs due to the strong interaction between DOX and the porous carrier. Additionally, the cell viability is decreased with the increase of the concentration. When the concentration is

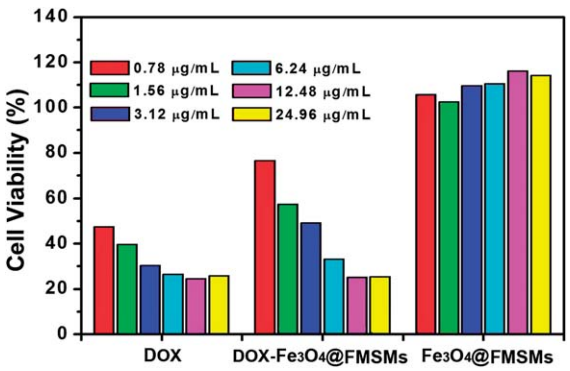

Fig. 10 Cell viability of L929 fibroblast cells incubated with DOX, DOX–Fe_3O_4/FMSMs and Fe_3O_4/FMSMs.

raised to a higher level (12.48, 24.96 μg mL^{-1}), DOX–Fe_3O_4/FMSMs display a high cytotoxicity to the fibroblast cells, which is similar to that of the free DOX. This can be explained by the following: free DOX molecules are transported into cells by a passive diffusion mechanism, while DOX–Fe_3O_4/FMSMs are captured by L929 fibroblast cells by a possible endocytosis mechanism and the DOX molecules are gradually released, as shown in the *in vitro* drug release results. This is in agreement with previous observations.[23] The results reveal that DOX–Fe_3O_4/FMSMs inhibit the proliferation of the cells to a great extent, suggesting its potential application for targeted cancer therapy.

4. Conclusions

In summary, we have designed a novel, fibrous-structured magnetic and mesoporous composite with spherical morphology *via* a facile and economical self-assembled process. In the self-assembled process, oleate-capped Fe_3O_4 nanocrystals with a uniform diameter of 9 nm were used directly without modifications. The results reveal that the novel material exhibits typical mesoporous structure, large pore size, good monodispersity, and superparamagnetic features. The *in vitro* and intracellular delivery of DOX studies showed that the material has a significantly prolonged circulation time and enhanced drug accumulation in the tumor. CLSM images indicate that the DOX-loaded composite could deliver DOX into the nuclei of HeLa cells to kill cells. Also, MTT assay reveals that the DOX-loaded sample leads to pronounced and efficient cytotoxic effects to L929 fibroblast cells, even similar to that of free DOX at high concentrations. Notably, the pure carrier is non-toxic up to all tested concentrations. The results suggest that the material has good potential for targeted cancer therapy.

Acknowledgements

This project is financially supported by National Basic Research Program of China (2007CB935502, 2010CB327704), and the National Natural Science Foundation of China (NSFC 20871035, 50702057, 50872131, 20901074, 20921002).

Notes and references

1 (*a*) J.-M. Nam, C. S. Thaxton and C. A. Mirkin, *Science*, 2003, **301**, 1884; (*b*) L. Gao, J. Wu, S. Lyle, K. Zehr, L. Cao and D. Gao, *J. Phys. Chem. C*, 2008, **112**, 17357; (*c*) L. Z. Gao, J. Zhuang, L. Nie, J. B. Zhang, Y. Zhang, N. Gu, T. H. Wang, J. Feng, D. L. Yang, S. Perrett and X. Y. Yan, *Nat. Nanotechnol.*, 2007, **2**, 577.

2 (*a*) P. S. Doyle, J. Bibette, A. Bancaud and J. L. Viovy, *Science*, 2002, **295**, 2237; (*b*) Y. Li, B. Yan, C. H. Deng, W. J. Yu, X. Q. Xu and P. Y. Yang, *Proteomics*, 2007, **7**, 2330; (*c*) D. Wang, J. He, N. Rosenzweig and Z. Rosenzweig, *Nano Lett.*, 2004, **4**, 409.

3 R. Abu-Reziq, H. Alper, D. G. Wan and M. L. Post, *J. Am. Chem. Soc.*, 2006, **128**, 5279.

4 Y. F. Zhu, S. Kaskel, J. Shi, T. Wage and K.-H. Van Pée, *Chem. Mater.*, 2007, **19**, 6408.

5 (*a*) P. P. Yang, Z. W. Quan, Z. Y. Hou, C. X. Li, X. J. Kang, Z. Y. Cheng and J. Lin, *Biomaterials*, 2009, **30**, 4786; (*b*) M. Arruebo, M. Galan, N. Navascues, C. Tellez, C. Marquina, M. R. Ibarra and J. Santamaria, *Chem. Mater.*, 2006, **18**, 1191; (*c*) S. Mornet, S. Vasseur, F. Grasnet and E. Duguet, *J. Mater. Chem.*, 2004, **14**, 2161; (*d*) W. Zhao, J. Gu, L. Zhang, H. Chen and J. Shi, *J. Am. Chem. Soc.*, 2005, **127**, 8916.

6 (*a*) J. B. Lian, X. C. Duan, J. M. Ma, P. Peng, T. Kim and W. J. Zheng, *ACS Nano*, 2009, **3**, 3749; (*b*) L. Y. Chen, Z. Lin, C. L. Zhao, Y. Y. Zheng, Y. Zhou and H. Peng, *J. Alloys Compd.*, 2011, **509**, L1; (*c*) Z. B. Huang and F. Q. Tang, *J. Colloid Interface Sci.*, 2005, **281**, 432; (*d*) S. H. Liu, R. M. Xing, F. Lu, R. K. Rana and J. J. Zhu, *J. Phys. Chem. C*, 2009, **113**, 21042; (*e*) J. G. Yu, X. X. Yu, B. B. Huang, X. Y. Zhang and Y. Dai, *Cryst. Growth Des.*, 2009, **9**, 1474.

7 (*a*) E. Ruiz-Hernandez, A. Lopez-Noriega, D. Arcos, I. Izquierdo-Barba, O. Terasaki and M. Vallet-Regı, *Chem. Mater.*, 2007, **19**, 3455; (*b*) J. Zhou, W. Wu, D. Caruntu, M. Yu, A. Martin, J. Chen, C. O'Connor and W. Zhou, *J. Phys. Chem. C*, 2007, **111**, 17473.

8 (*a*) S. L. Gai, P. P. Yang, C. X. Li, W. X. Wang, Y. L. Dai, N. Niu and J. Lin, *Adv. Funct. Mater.*, 2010, **20**, 1166; (*b*) Y. F. Zhu, T. Ikoma, N. Hanagata and S. Kaskel, *Small*, 2010, **6**, 471; (*c*) M. Liong, J. Lu, M. Kovochich, T. Xia, S. G. Ruehm, A. E. Nel, F. Tamanoi and J. I. Zink, *ACS Nano*, 2008, **2**, 889; (*d*) L. Zhang, S. Z. Qiao, Y. G. Jin, Z. G. Chen, H. C. Gu and G. Q. Lu, *Adv. Mater.*, 2008, **20**, 805.

9 (*a*) X. P. Dong, H. R. Chen, W. R. Zhao, X. Li and J. L. Shi, *Chem. Mater.*, 2007, **19**, 3484; (*b*) A. B. Fuertes, T. Valdes-Solis, M. Sevilla and P. Tartaj, *J. Phys. Chem. C*, 2008, **112**, 3648.

10 (*a*) T. K. Jain, M. A. Morales, S. K. Sahoo, D. L. Leslie-Pelecky and V. Labhasetwar, *Mol. Pharmaceutics*, 2005, **2**, 194; (*b*) J. L. Zhang, R. S. Srivastava and R. D. K. Misra, *Langmuir*, 2007, **23**, 6342.

11 V. M. D. Paoli, S. H. D. P. Lacerda, L. Spinu, B. Ingber, Z. Rosenzweig and N. Rosenzweig, *Langmuir*, 2006, **22**, 5894.

12 L. O. Cinteza, T. Y. Ohulchanskyy, Y. Sahoo, E. J. Bergey, R. K. Pandey and P. N. Prasad, *Mol. Pharmaceutics*, 2006, **3**, 415.

13 (*a*) P. P. Yang, Z. W. Quan, L. L. Lu, S. S. Huang and J. Lin, *Biomaterials*, 2008, **29**, 692; (*b*) N. K. Mal, M. Fujiwara and Y. Tanaka, *Nature*, 2003, **421**, 350; (*c*) V. Polshettiwar, D. Cha, X. Zhang and J. M. Basset, *Angew. Chem., Int. Ed.*, 2010, **49**, 9652; (*d*) J. Lu, M. Liong, J. I. Zink and F. Tamanoi, *Small*, 2007, **3**, 1341; (*e*) B. G. Trewyn, I. I. Slowing, S. Giri, H.-T. Chen and V. S.-Y. Lin, *Acc. Chem. Res.*, 2007, **40**, 846.

14 (*a*) J. Park, K. An, Y. Hwang, J.-G. Park, H.-J. Noh, J.-Y. Kim, J.-H. Park, N.-M. Hwang and T. Hyeon, *Nat. Mater.*, 2004, **3**, 891; (*b*) G. H. Gao, X. H. Liu, R. R. Shi, K. C. Zhou, Y. G. Shi, R. Z. Ma, E. Takayama-Muromachi and G. Z. Qiu, *Cryst. Growth Des.*, 2010, **10**, 2888; (*c*) T. Hyeon, S. S. Lee, J. Park, Y. Chung and H. B. Na, *J. Am. Chem. Soc.*, 2001, **123**, 12798; (*d*) S. Sun and H. Zeng, *J. Am. Chem. Soc.*, 2002, **124**, 8204; (*e*) N. R. Jana, Y. Chen and X. Peng, *Chem. Mater.*, 2004, **16**, 3931.

15 (*a*) T. R. Zhang, J. P. Ge, Y. X. Hu and Y. D. Yin, *Nano Lett.*, 2007, **7**, 3203; (*b*) W. C. W. Chan and S. M. Nie, *Science*, 1998, **281**, 2016; (*c*) M. Kim, Y. Chen, Y. Liu and X. Peng, *Adv. Mater.*, 2005, **17**, 1429.

16 (*a*) G.-S. Yi and G.-M. Chow, *Chem. Mater.*, 2006, **19**, 341; (*b*) J. Kim, H. S. Kim, N. Lee, T. Kim, H. Kim, T. Yu, I. C. Song, W. K. Moon and T. Hyeon, *Angew. Chem.*, 2008, **120**, 8566.

17 (*a*) H. S. Qian, H. C. Guo, P. C.-L. Ho, R. Mahendran and Y. Zhang, *Small*, 2009, **5**, 2285; (*b*) Y.-S. Lin, S.-H. Wu, Y. Hung, Y.-H. Chou, C. Chang, M.-L. Lin, C.-P. Tsai and C.-Y. Mou, *Chem. Mater.*, 2006, **18**, 5170; (*c*) J. P. Yang, Y. H. Deng, Q. L. Wu, J. Zhou, H. F. Bao, Q. Li, F. Zhang, F. Y. Li, B. Tu and D. Y. Zhao, *Langmuir*, 2010, **26**, 8850; (*d*) Y. S. Lin and C. L. Haynes, *Chem. Mater.*, 2009, **21**, 3979.

18 (*a*) C. Y. Lai, B. G. Trewyn, D. M. Jeftinija, K. Jeftinija, S. Xu, S. Jeftinija and V. S. Y. Lin, *J. Am. Chem. Soc.*, 2003, **125**, 4451; D. R. Radu, C.-Y. Lai, K. Jeftinija, E. W. Rowe, S. Jeftinija and V. S.-Y. Lin, *J. Am. Chem. Soc.*, 2004, **126**, 13216.

19 J. Crown, V. Dieras, M. Kaufmann, G. von Minckwitz, S. Kaye, R. Leonard, M. Marty, J.-L. Misset, B. Osterwalder and M. Piccart, *Lancet Oncol.*, 2002, **3**, 719.

20 (*a*) A. S. M. Chong and X. S. Zhao, *J. Phys. Chem. B*, 2003, **107**, 12650; (*b*) D. W. Sindorf and G. E. Maciel, *J. Am. Chem. Soc.*, 1983, **105**, 3767; (*c*) E. Lindner, T. Schneller, F. Auer and H. A. Mayer, *Angew. Chem., Int. Ed.*, 1999, **38**, 2155.

21 (*a*) A. Jitianu, M. Crisan, A. Meghea, I. Rau and M. Zaharescu, *J. Mater. Chem.*, 2002, **12**, 1401; (*b*) M. Yu, J. Lin and J. Fang, *Chem. Mater.*, 2005, **17**, 1783.

22 (*a*) L. S. del Rosario, B. Demirdirek, A. Harmon, D. Orban and K. E. Uhrich, *Macromol. Biosci.*, 2010, **10**, 415; (*b*) G. Minotti, P. Menna, E. Salvatorelli, G. Cairo and L. Gianni, *Pharmacol. Rev.*, 2004, **56**, 185.

23 (*a*) Y. Hu, Y. Ding, D. Ding, M. J. Sun, L. Y. Zhang, X. Q. Jiang and C. Z. Yang, *Biomacromolecules*, 2007, **8**, 106; (*b*) E. R. Gillies and J. M. J. Frechet, *Bioconjugate Chem.*, 2005, **16**, 361.

